Received: 23 October 2019 | Revised: 27 November 2019 | Accepted: 27 November 2019

DOI: 10.1096/fj.201902588R

RESEARCH ARTICLE

THE FASEB JOURNAL

Demyelinating polyneuropathy in goats lacking prion protein

Fredrik S. Skedsmo[1] | Giulia Malachin[2] | Dag Inge Våge[3] | Mie Marie Hammervold[3] | Øyvind Salvesen[4] | Cecilie Ersdal[4] | Birgit Ranheim[4] | Marit H. Stafsnes[5] | Zdenka Bartosova[5] | Per Bruheim[5] | Karin H. Jäderlund[1] | Kaspar Matiasek[6] | Arild Espenes[2] | Michael A. Tranulis[2]

[1]Department of Companion Animal Clinical Sciences, Faculty of Veterinary Medicine, Norwegian University of Life Sciences, Oslo, Norway

[2]Department of Basic Sciences and Aquatic Medicine, Faculty of Veterinary Medicine, Norwegian University of Life Sciences, Oslo, Norway

[3]Centre for Integrative Genetics (CIGENE), Department of Animal and Aquacultural Sciences, Faculty of Biosciences, Norwegian University of Life Sciences, Ås, Norway

[4]Department of Production Animal Clinical Sciences, Faculty of Veterinary Medicine, Norwegian University of Life Sciences, Oslo, Norway

[5]Department of Biotechnology and Food Science, Faculty of Natural Sciences, Norwegian University of Science and Technology, Trondheim, Norway

[6]Section of Clinical & Comparative Neuropathology, Centre for Clinical Veterinary Medicine, Ludwig-Maximilians-Universität, Munich, Germany

Correspondence
Michael A. Tranulis, Department of Basic Sciences and Aquatic Medicine, Faculty of Veterinary Medicine, Norwegian University of Life Sciences, Ullevålsveien 72, Oslo 0454, Norway.
Email: Michael.Tranulis@nmbu.no

Abstract

Studies in mice with ablation of *Prnp*, the gene that encodes the cellular prion protein (PrP^C), have led to the hypothesis that PrP^C is important for peripheral nerve myelin maintenance. Here, we have used a nontransgenic animal model to put this idea to the test; namely, goats that, due to a naturally occurring nonsense mutation, lack PrP^C. Teased nerve fiber preparation revealed a demyelinating pathology in goats without PrP^C. Affected nerves were invaded by macrophages and T cells and displayed vacuolated fibers, shrunken axons, and onion bulbs. Peripheral nerve lipid composition was similar in young goats with or without PrP^C, but markedly different between corresponding groups of adult goats, reflecting the progressive nature of the neuropathy. This is the first report of a subclinical demyelinating polyneuropathy caused by loss of PrP^C function in a nontransgenic mammal.

KEYWORDS

lipidomic, myelin, neuropathy, PRNP haplotype

Abbreviations: AI bucks, Selected bucks used in artificial insemination (AI) in the Norwegian goat population; BSA, Bovine serum albumin; HexCer, Hexosyl ceramides; MAF, Minimal allele frequency; PBS, Phosphate-buffered saline; $PRNP^{Ter/Ter}$, Goats homozygous for nonsense mutation in *PRNP*; PrP^{Sc}, Misfolded prion protein; PrPC, Cellular prion protein; *Prnp*, *PRNP*, Gene encoding the cellular prion protein; SNP, Single-nucleotide polymorphism; TBST, Tris-buffered saline-Tween.

Fredrik S. Skedsmo and Giulia Malachin joint first authors.

Funding information
The Research Council of Norway, Grant/Award Number: 227386/E40

1 | INTRODUCTION

Prion diseases are rare, invariably fatal, neurodegenerative conditions in which pathognomonic misfolded prion protein (PrP^{Sc}) aggregates appear in the central nervous system of affected humans and animals.[1] The misfolded PrP^{Sc} conformers stem from physiological cellular prion protein (PrP^{C}), which, in an incompletely understood process, is converted to PrP^{Sc} through physical interaction between the two conformational states of PrP. Transgenic mice without endogenous PrP^{C} cannot develop prion disease.[2,3] Thus, neuronal PrP^{C} is the obligatory molecule for prion disease progression and hence is the prime target for interventions.

Several lines of transgenic mice with ablation of gene encoding the cellular prion protein *(Prnp)* have been generated (hereafter referred to as $Prnp^{-/-}$), and only minor abnormalities were initially observed under resting conditions.[3-8] However, Nishida and coworkers reported white matter vacuolation, demyelination, and a loss of large myelinated fibers in peripheral nerves in several $Prnp^{-/-}$ lines of mice, and proposed that PrP^{C} serves important roles in myelin formation and/or maintenance in both the central and peripheral nervous system.[9] After a period of relative neglect, the topic of PrP^{C} and myelin health has recently been revisited in a series of investigations involving several experimental designs and $Prnp^{-/-}$ mouse lines.[10] The current view is that axonal PrP^{C} contributes to preserve Schwann cell myelin quality. Specifically, PrP^{C}-derived peptides, liberated from axons through controlled proteolysis, diffuse to Schwann cell receptors and thereby stimulate myelin maintenance.[11] Absence of such signalling gradually leads to demyelination and remyelination in response.

Different from inbred laboratory mice, dairy goats, and humans have a high degree of genetic variation. By comparing *PRNP* haplotypes with and without the $PRNP^{Ter}$ nonsense mutation, we find that the region affected by genetic hitchhiking is surprisingly short, covering less than 1% of genes encoded by chromosome 13. Like $Prnp^{-/-}$ mice, goats without PrP^{C} develop a mild demyelinating neuropathy, demonstrating that PrP^{C} functions in myelin maintenance are highly conserved and probably translates to other mammals, including humans.

2 | MATERIALS AND METHODS

2.1 | Animals and ethics

Animal experiments and tissue sampling were performed in compliance with the ethical guidelines and approved by the Norwegian Animal Research Authority (FOTS ID 7860, 5826), with reference to the Norwegian regulations on animal experimentation. All goats were of the Norwegian Dairy Goat Breed, recruited from a research facility at the Norwegian University of Life Sciences and housed together in a farmhouse environment.

For morphological analyses, electrophysiology and lipidomics, a total of 24 goats were used, of which 10 were homozygous for the wild type *PRNP* allele and 14 were homozygous for the mutated *PRNP* allele (hereafter called $PRNP^{+/+}$ and $PRNP^{Ter/Ter}$, respectively). Genomic DNA

TABLE 1 Antibodies and dilutions used in the analyses

Name	Catalogue No.	Producer	Dilutions		
			IHC	IF	WB
Anti-Iba1	019-19741	Fujifilm Wako Chemicals, Neuss, Germany	1/250	NA	NA
Anti-CD3	A-0452	Dako, California, United States	1/500	NA	NA
Anti-PrP 6H4	01-010	Prionics, Zürich, Switzerland	NA	1/500	NA
Anti-PrP P4	R8007	Ridascreen Biopharm, Darmstadt, Germany	NA	NA	1/100
Anti-Neurofilament 200	064H-4809	Sigma-Aldrich, Merck, Darmstadt, Germany	NA	1/400	NA

Abbreviations: NA = Not analyzed. IHC immunohistochemistry, IF immunofluorescence, WB western blot.

sampled for haplotype analysis is specified below. A detailed overview of goats used, according to age groups and analyses, is given in Supplementary Table 1.

2.2 | Tissue sampling

Tissues were collected immediately after euthanasia. Samples for immunohistochemistry were fixed in 10% neutral buffered formalin and then embedded in paraffin. For western blot, samples were snap frozen in isopentane, transferred to liquid nitrogen, and stored at −80°C. Whole-trunk samples of peripheral nerves were gently separated into fascicles and fixed in 2.5% glutaraldehyde in Soerensen's phosphate buffer (0.1 M, pH 7.4) for 4 hours at room temperature and then overnight at 4°C.

2.3 | Immunohistochemistry

Sections of 3-4 μm were placed on glass slides (Superfrost Plus®, Menzel Gläser, Thermo Fisher Scientific, Massachusetts, United States) and stored at 4°C until staining. The slides were deparaffinized in xylene and rehydrated through a descending alcohol series. Between steps, sections were washed twice in phosphate-buffered saline (PBS) for 5 minutes. For anti-Iba1, the slides were incubated with trypsin (1 mg/mL) in Tris HCl (0.1 M, pH 8 with 0.1% $CaCl_2$) for 40 min at 37°C before inhibition of endogenous peroxidase. For anti-CD3, antigen retrieval was performed by heating the slides in Tris/EDTA (pH 9.1) in a microwave before inhibition. The temperature in the solution was held at 92°C degrees for 5 min, thereafter the slides were kept in the hot solution for another 5 min before the procedure was repeated. Endogenous peroxidase was inhibited with 3% H_2O_2 in methanol for 10 minutes. Nonspecific antibody binding was blocked by incubating the slides for 20 minutes in 5% bovine serum albumin (BSA) with 2% goat serum. The sections were incubated for 60 min with primary antibodies, diluted in 1% BSA at dilutions indicated in Table 1. Next, the sections were incubated with secondary antibodies conjugated to horseradish peroxidase-labelled polymer from the EnVision+ kit (catalogue number K4009, Dako, California, United States) for 30 minutes, and developed with AEC+-substrate for 5 minutes. The sections were counterstained with hematoxylin and mounted with Aquatex (Merck, Darmstadt, Germany). Sections for which the primary antibodies were omitted were used as negative controls. Micrographs were taken using Axio Imager 2 microscope, equipped with an Axiocam 506 color camera (Zeiss, Oberkochen, Germany). The level of immune cell influx in peripheral nerves was scored from zero to three (0 = negative, 1 = low, 2 = moderate, and 3 = high) by two independent observers and an average was calculated. Slide-labels were concealed prior to scoring.

2.4 | Immunofluorescence

Cryostat sections of 8 μm were placed on glass slides (Superfrost Plus) and stored at −80°C until staining. After thawing, slides were fixed in formal-calcium (4% formaldehyde, 1% calcium chloride, pH 7.44) for 15 minutes. Blocking was performed for 30 minutes in 5% BSA with 2% goat serum followed by incubation with primary antibodies overnight at 4°C, diluted in blocking solution at dilutions specified in Table 1. Slides were incubated with secondary antibodies, goat anti-mouse IgG1 Alexa Fluor 488 and goat anti-rabbit IgG Alexa Fluor 594 (both from Invitrogen, Thermo Fisher Scientific), diluted in PBS for 45 minutes. The slides were mounted with ProLong Gold Antifade Mountant with 4′,6 diamidino-2-phenyl indole (DAPI; Molecular Probes, Thermo Fisher Scientific). Micrographs were taken using Axio Imager 2 microscope, equipped with an Axiocam 506 mono camera (Zeiss).

2.5 | Western blot

Peripheral nerves were lysed in homogenizer buffer (Tris HCl 50 μM, NaCl 150 mM, EDTA 1mM, DOC 0.25%, NP40 1%), supplemented with protease inhibitor cocktail (Complete, Roche, Merck), after removal of the connective tissue. Protein concentration was measured with the Protein assay (Bio-Rad, Hercules, California, USA). Total proteins (80 μg) were deglycosylated with PNGase-F, according to manufacturer's instructions (New England Biolabs, Ipswich, Massachusetts, United States). One hundred and thirty micrograms of total proteins and 80 μg of the deglycosylated samples were separated on SDS-Page (12% Bio-Rad) and blotted on PVDF membrane (GE Healthcare, Little Chalfont, United Kingdom). After protein transfer, gels were stained with Coomassie blue (Invitrogen, Thermo Fisher Scientific). Membranes were blocked in 5% dry milk in Tris-buffered saline-Tween (TBST), and probed with primary antibody Anti-PrP P4, diluted as indicated in Table 1. Secondary anti-mouse antibody conjugated with alkaline phosphatases was used for the detection. The signal was developed with Enhanced chemiluminescence (ECF) reagent (GE Healthcare) and Typhoon 9200 (Amersham Bioscience, GE Healthcare).

2.6 | Processing of peripheral nerves for morphological assessment

About 1-2 mm pieces were cut from the nerve fascicles, postfixed in 1% osmium tetroxide at 4°C, and transferred to washing buffer. The samples were dehydrated through an ascending acetone series and embedded in epoxy (Electron Microscopy Sciences, Hatfield, Pennsylvania, United States). Semi-thin (0.5 μm) sections were stained with toluidine blue and safranin-O, and evaluated by light microscopy using a

Zeiss Axio Imager 2 microscope equipped with an Axiocam 506 color camera. Ultra-thin (70 nm) sections were contrasted with uranyl acetate and lead citrate, and studied using a FEI Morgagni 268 transmission electron microscope (FEI, Hillsboro, Oregon, United States) equipped with an Olympus Veleta CCD camera. In the semi-thin sections, the number of nuclei per 0.5 mm^2 from each individual was quantified independently by two observers.

For nerve fiber teasing, 1 cm pieces of fixed nerve fascicles were postfixed in 2% osmium tetroxide at room temperature for 1 hours, washed in phosphate buffer, immersed in glycerol and separated under a dissection microscope. A total of 489 teased nerve fibers were studied; 313 from goats homozygous for nonsense mutation in *PRNP* (*PRNP*$^{Ter/Ter}$) goats and 176 from *PRNP*$^{+/+}$ goats. The percentage of fibers with evidence of demyelination and/or remyelination (internodes with reduced length and myelin thickness) was scored blindly by two independent observers.

For morphometric analysis, semi-thin sections were analyzed with Image-Pro Plus software (Media cybernetics, Maryland, USA). The area of the myelin sheaths and axons were measured and used to calculate the respective diameters as previously described.[12] *G*-ratio was then calculated as the ratio between axonal diameter and fiber diameter.

2.7 | Extraction of lipids from peripheral nerves

Mass spectrometry grade water and chloroform (reagent Ph. Eur.) stabilized with 0.6% of ethanol were purchased from VWR International (Radnor, Pennsylvania, United States). Methanol (LC-MS grade) was obtained from Merck. Ammonium acetate (for mass spectrometry, 98%) was purchased from Honeywell International Inc (Charlotte, North Carolina, United States).

Lipids from goat nerve tissue were extracted using the solvent system based on the Folch method.[13] A Precellys®24 bead homogenizer equipped with a Cryolys temperature controller (All Bertin Technologies SAS, Montigny-Le-Bretonneux, France) was used to disrupt and homogenize the tissue for lipid extraction. Nerve tissue (50 mg) was homogenized with zirconium oxide beads (0.5 ± 0.01 g, Ø 1.4 mm) in 500 µL of a cold mixture of chloroform/methanol (2:1, v/v). The tissue was kept frozen during cutting and weighing. Final rounds[5-10] of bead-beating for 30 seconds at 6500 rpm, with an intermediate 15 seconds pause between rounds were performed. Another 500 µL of a cold mixture of chloroform/methanol (2:1, v/v) was added to the sample and the tube was shaken for 10 minutes using a thermoshaker (Thermal shake lite, VWR) and phase separation was induced by adding 200 µL of 20 mM acetic acid. After 10 minutes of shaking (1500 rpm, 16°C), tubes were centrifuged for 6 minutes at maximum speed (13 400 rpm) using a small centrifuge (MiniSpin, Eppendorf, Hamburg, Germany). A volume of 400 µL of the chloroform layer (lower) was collected and the sample re-extracted with 500 µL of a cold mixture of chloroform/methanol/water (86:14:1, v/v), vortexed and centrifuged as above. From the lower layer, 650 µL was collected and pooled with the first extract. The resulting extract was filtered through a syringe filter with GHP membrane (0.2 µm, Ø 13 mm, Acrodisc®, Pall Laboratory, Port Washington, New York, United States) and kept at −20°C until analysis with ultra-performance convergence chromatography tandem mass spectrometry (UPC^2-MS/MS). Dichloromethane was used as diluent for lipid extracts.

2.8 | Chromatographic analysis of lipids

A lipid profile analysis was performed using an UPC^2® separation system coupled to a hybrid quadrupole orthogonal time-of-flight mass spectrometer SYNAPT G2-S HDMS (Waters, Milford, Massachusetts, United States). A previously described analytical method[14] was adopted and modified. The column was protected with a VanGuard pre-column (BEH 2.1 × 5 mm) and temperature of the column was 50°C. The gradient of the modifier used was set as follows: 0 minutes, 1%; 4.0 minutes, 30%;[6] 4.4 minutes, 50%;[2] 6.25 minutes, 50%;[1] 7.25 minutes, 50%;[6] 7.35 minutes, 1%[6], 8.50 minutes, 1%.

The mass spectrometer was operated in MS^E mode and the collision energy ramped from 20 to 30 eV for positive ion mode and from 20 to 35 eV for negative ion mode. Data were acquired over the mass range of 50-1200 Da and the resolution of the mass spectrometer was 20 000. Both positive and negative ion electrospray ionization modes were applied. MS tuning parameters were set as follows: capillary voltages 3.0 kV and −2.5 kV for positive and negative ionization modes, respectively; source temperature 150°C; the sampling cone 40V; source offset 60V; desolvation temperature 500°C; cone gas flow 50 L/h; desolvation gas flow 850 L/h; nebulizer gas pressure 4 bar. Leucine enkephalin was used as the lock mass. Identification of a lipid compound is based on the following main characteristics: retention time of the appropriate lipid class, accurate mass (ppm error <5), isotope pattern similarity (>80%), and fragmentation pattern. The lipid nomenclature and shorthand notation described by LIPID MAPS[15] and Liebisch G. et al,[16] were followed.

2.9 | Haplotype analysis

A total of 48 goats, either heterozygous (n = 27) or homozygous (n = 21), were used for the haplotype analysis (henceforth referred to as *PRNP*$^{+/Ter}$ and *PRNP*$^{Ter/Ter}$ respectively). A previously acquired Illumina 50K SNP(single-nucleotide polymorphism) dataset of 48 AI bucks (born 2009-2012)

from the Norwegian goat breeding system was used as a reference population. Among the 48 bucks, 41 were wild type ($PRNP^{+/+}$), and 7 were heterozygous, while none were homozygous $PRNP^{Ter/Ter}$. The goats were genotyped by the Illumina 50K SNP (single-nucleotide polymorphism) chip. The genotyping was carried out by Neogen Ltd, Scotland, UK.

After initial filtering for quality of the *PRNP*-groups, the final number of markers were 49 277. Two individuals (one $PRNP^{+/Ter}$ and one $PRNP^{Ter/Ter}$) were removed due to low call rate. The 48 AI bucks previously genotyped with the same SNPs array were left with 49 124 markers after identical quality filtering. Comparing these two datasets after filtering, 47 847 markers were present in both datasets. These two datasets were merged into one common file, containing 94 individuals and the 47 847 markers.

SNP (single-nucleotide polymorphism) positions were updated to the ARS1 assembly version. The minor allele frequencies (MAF) for all SNPs on chromosome 13 were calculated using the PLINK −freq function. This analysis was done for the three genotype classes separately ($PRNP^{+/+}$, $PRNP^{+/Ter}$ and $PRNP^{Ter/Ter}$). The seven heterozygous AI bucks were included in the $PRNP^{+/Ter}$ group. In addition, the average MAF of all chromosomes were estimated for the same genotype classes.

2.10 | Electrophysiological recordings and clinical examination

All electrophysiological recordings were conducted in the same rooms as the goats were housed. The goats were placed in a small pen and restrained using a halter and rope. The experimental session was conducted on the thoracic limb in every animal. Self-adhesive surface stimulation electrodes (Neuroline 70010-K/C/12, AMBU, Copenhagen, Denmark) were attached to the skin overlaying the lateral digital nerves after shaving and washing with ether and ethanol. Recording needle electrodes (Aiglette 019200 REF:S46-638, Technomed, Netherlands) were placed in the ipsilateral deltoid muscle, and a reference electrode (Natus Ref 019-409100, Middleton, Wisconsin, United States) was placed on the back of the goat. Flexible leads were connected to the electrodes and resistance of each electrode pair was checked to be below 3 kΩ.

Stimulations and recordings were performed using Cephalon Natus Viking Quest (Cephalon, Aalborg, Denmark). Stimulation started at 1 mA and increments were in steps of 0.5 mA. Reactions to the stimulation were assessed and scored according to the following descriptors: 0 = no reaction; 1 = weak muscle contraction of the deltoid muscle; 2 = muscle contraction of the deltoid muscle and a short withdrawal reflex; 3 = definite withdrawal reflex and muscle contractions in the flank; 4 = distinct and repeated withdrawal reflex accompanied by responses in other body parts (head, neck, contralateral leg); 5 = distinct and repeated withdrawal reflex accompanied with a whole body response.

A standard single stimulus consisted of a train-of-five 1 ms constant current pulses delivered at 200 Hz. The electromyography (EMG) activity in the deltoid muscle was recorded from 100 ms before to 300 ms after each stimulus. Reflex amplitude was calculated as the root-mean square (RMS) of the EMG burst activity following stimulation. To be considered a reflex response, the EMG burst following the electrical stimulation had to have a RMS amplitude of at least 30 μV, with a minimal duration of 20 ms. Latency was defined as the time (ms) from the stimulus to the onset of the EMG deflection. The lowest stimulation intensity eliciting an EMG response combined with a behavioral reaction score > 2 was used when latency was measured.

$PRNP^{Ter/Ter}$ goats were subjected to clinical, including basic neurological, examination.

2.11 | Statistical analysis

Data were processed using GraphPad Prism. For statistical comparison of two groups ($PRNP^{+/+}$ and $PRNP^{Ter/Ter}$) for demyelinated fibers, number of nuclei in semi-thin sections and *g*-ratio we performed unpaired *t*-tests.

For haplotype analysis, the following filtering parameters were used; call rate > 90% both for individual markers and per animal, maf > 1% and hwe *P* value > 1e-5, using the PLINK 2.0 software (−geno, −mind, −maf, and −hwe).[17]

Mass chromatogram raw data were processed using Progenesis QI software (Nonlinear Dynamics, Waters) with in-built LipidBlast[18] and LipidMaps databases[19] for lipid identification. Lipid classification was based on defined retention time windows and experimentally obtained response factors.[20] Only lipid species within the defined lipid class retention time windows were retained for analysis and interpretation (Supplementary Table 4). Further, the processed data were exported for multivariate analysis using a freely available statistical tool MetaboAnalyst.[21] The data were normalized and auto-scaled before they were subjected to principal component analysis (PCA) and hierarchical clustering analysis (heatmap).

3 | RESULTS

3.1 | Morphological and immunohistochemical analyses of peripheral nerves

Teased fibers from the tibial nerve of the $PRNP^{Ter/Ter}$ goats (Figure 1 and 2A) had interposed, short internodes with

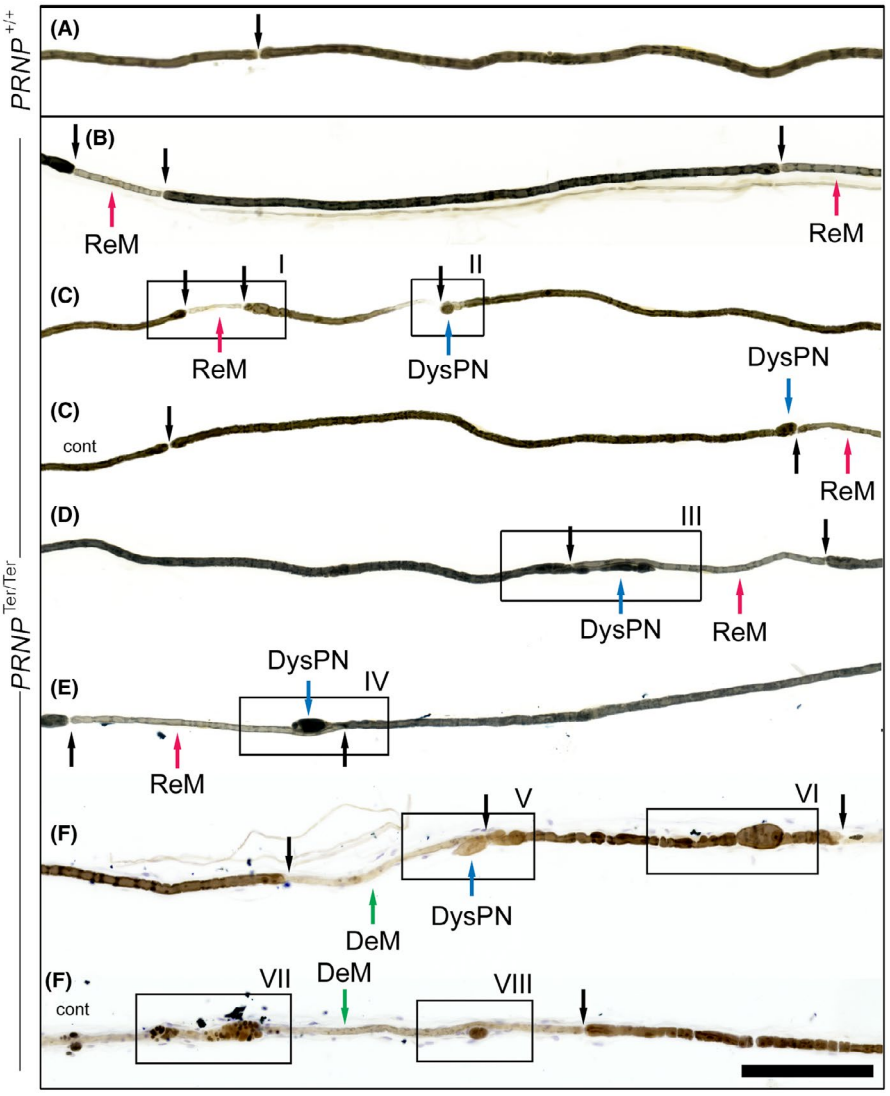

FIGURE 1 Teased nerve fibers. A, Nerve fiber from normal goat ($PRNP^{+/+}$); the thickness of the myelin is similar on both sides of the node of Ranvier (black arrow). B-F, Nerve fibers from $PRNP^{Ter/Ter}$ goats. Short internodes with reduced myelin thickness (intercalated internodes, red arrows) between (C, D, E) or at both sides (B) of longer internodes with normal myelin thickness. The intercalated internodes are associated with the presence of dysmorphic paranodes (blue arrows) (C-E). Active segmental demyelination (green arrows) with myelin degradation products along the demyelinated axon, and accompanied by cellular infiltrates (F). Black arrows = Nodes of Ranvier, ReM = Remyelinated segments, DeM = Demyelinating segments, DysPN = Dysmorphic paranodes. Black boxes and Roman numerals refer to segments shown at higher magnification in Figure 2. Bar 200 μm. Staining: Osmium tetroxide with (F) or without (A-E) hematoxylin

reduced myelin thickness, consistent with remyelination,[22] wide-spread multifocally. These segments intermingled with internodes of normal length and myelin thickness. More specifically, the remyelinated segments were frequently found as intercalated internodes at both sides of a longer internode with a thicker myelin sheath. The paranodes of the latter were often dysmorphic, with changes ranging from swollen paranodes to protrusions of the myelin sheath stretching for 100-200 μm along the intercalated internodes. Series of short, thinly myelinated internodes were also observed. Actively demyelinating segments with osmiophilic balls consisting of myelin debris[12] were accompanied by cellular infiltrates, but such segments were infrequently observed (Figure 1F). The $PRNP^{Ter/Ter}$ goats had an increased percentage of fibers ($P = .0001$), with evidence of demyelination and/or remyelination, compared with age-matched controls (Figure 2B). The changes in the 8 months old goats were less pronounced, but morphologically similar to those in adult (3-7 years) goats.

Semi-thin sections confirmed these morphological alterations (Figure 3), with the presence of thin myelin sheaths and onion bulbs (Figure 3E,G). Onion bulbs consist of concentrically arranged Schwann cell processes, and suggest repeated demyelination and remyelination. Vacuolated and thickened fibers were occasionally seen in the nerves of the $PRNP^{Ter/Ter}$ goats. These fibers presented with interlamellar myelin splitting (Figure 3D), thin myelin and/or hypertrophy of the Schwann cell adaxonal cytoplasm, often in combination with axonal shrinkage (Figure 3G). Diminished axonal diameters without other pathological features were present, but difficult to interpret, as apparent axonal retraction from the myelin sheath can be found artifactual. Paranodal outfoldings were identified in longitudinal sections (Figure 3H). The splitting of the myelin sheath in the $PRNP^{Ter/Ter}$ goats must be distinguished from the very prominent Schmidt-Lanterman clefts seen in both groups (Figure 3C).

Moreover, an increased number of mononuclear cells were observed evenly distributed in the endoneurial connective tissue of the $PRNP^{Ter/Ter}$ goats (Figure 3F, $P = .0267$). To investigate these cells, we stained nerve sections with antibodies against Iba1 (macrophages) and

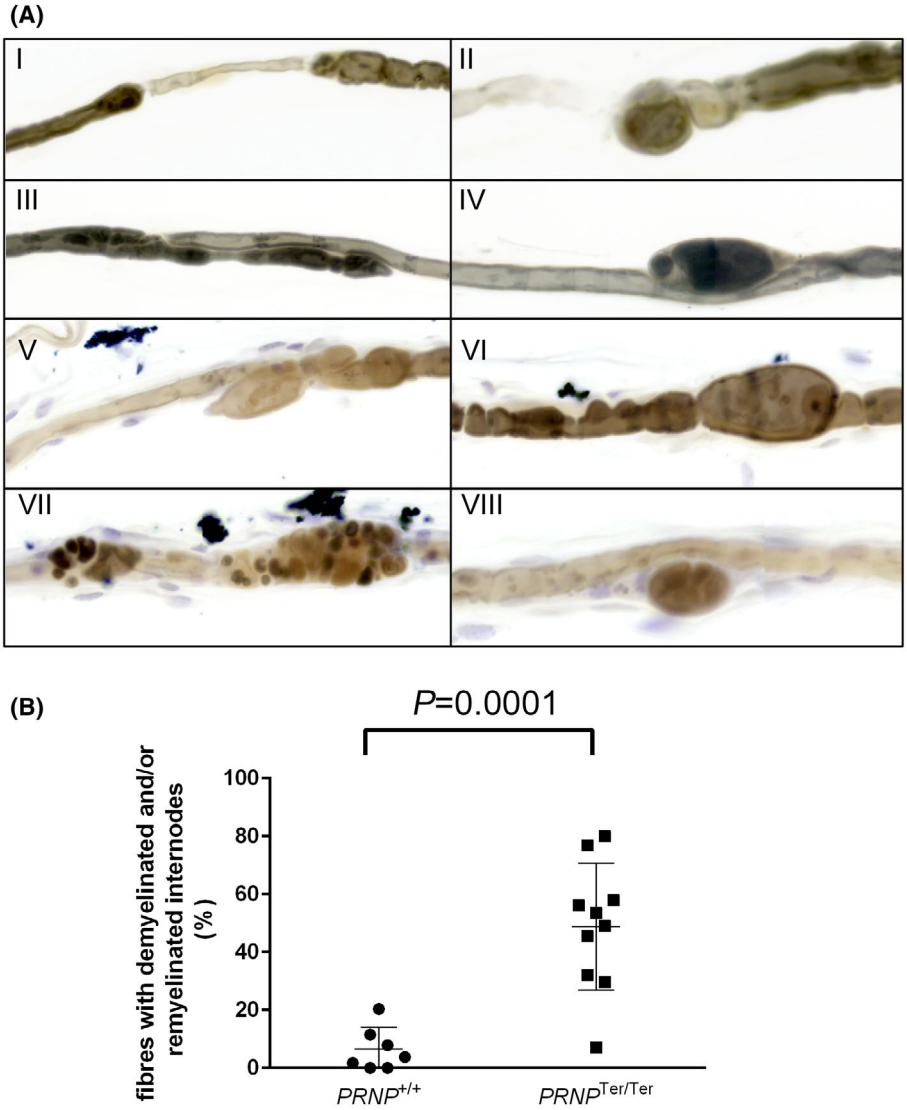

FIGURE 2 A, Higher magnification of changes in teased nerve fibers marked by black boxes in Figure 1. Intercalated, thinly myelinated and short internodes, indicative of paranodal demyelination and subsequent remyelination (I-IV). The paranodal pathology ranged from swollen paranodes (II) to outfoldings along the intercalated internode (III-V). Cellular infiltrates were visible along demyelinating segments (VI). Active demyelination in an internode exhibiting highly irregular myelin sheath with myelin degradation products and cellular infiltrates present along the demyelinating segment (VII, VIII). B, In *PRNP*$^{Ter/Ter}$ goats there were significantly more fibers with evidence of demyelination or remyelination than in normal goats

CD3 (T lymphocytes). This showed that both the number of macrophages (Figure 4A,B) and T lymphocytes (Figure 4C,D) were increased in the endoneurium of adult goats lacking PrP^{C}.

At the ultrastructural level, *PRNP*$^{Ter/Ter}$ fibers with myelin splitting proved to be fibers with intramyelinic edema (Figure 5A). The myelin splitting occurred at the intraperiod line (not shown), separating the outer aspects of the Schwann cell plasma membrane, thereby focally increasing the extracellular volume in the myelin sheath. In the fibers with swelling within the adaxonal and/or abaxonal Schwann cell cytoplasm, the edematous spaces contained vesicular structures, probably swollen organelles (Figures 5B and 6B,D). The corresponding axons were shrunken, with an increased density of neurofilaments (Figure 5B,C) and, occasionally, other organelles, suggesting compression[23] (Figure 5C). Myelinated fibers with thin myelin sheaths surrounded by supernumerary Schwann cells, recognized by the presence of a basal lamina, were present (Figure 5C). Cells without basal lamina, probably representing the Iba1- or CD3-positive cells demonstrated by immunohistochemistry, were observed around some of the nerve fibers (Figure 5D). Neither of these were observed to penetrate the basal lamina of the Schwann cell, nor did we observe such cells between the myelin sheath and axon. Less frequently, severely dysmorphic organelles were present in the adaxonal Schwann cell cytoplasm (Figure 5E). No changes were detected in unmyelinated C-fibers of Remak clusters (Figure 5F).

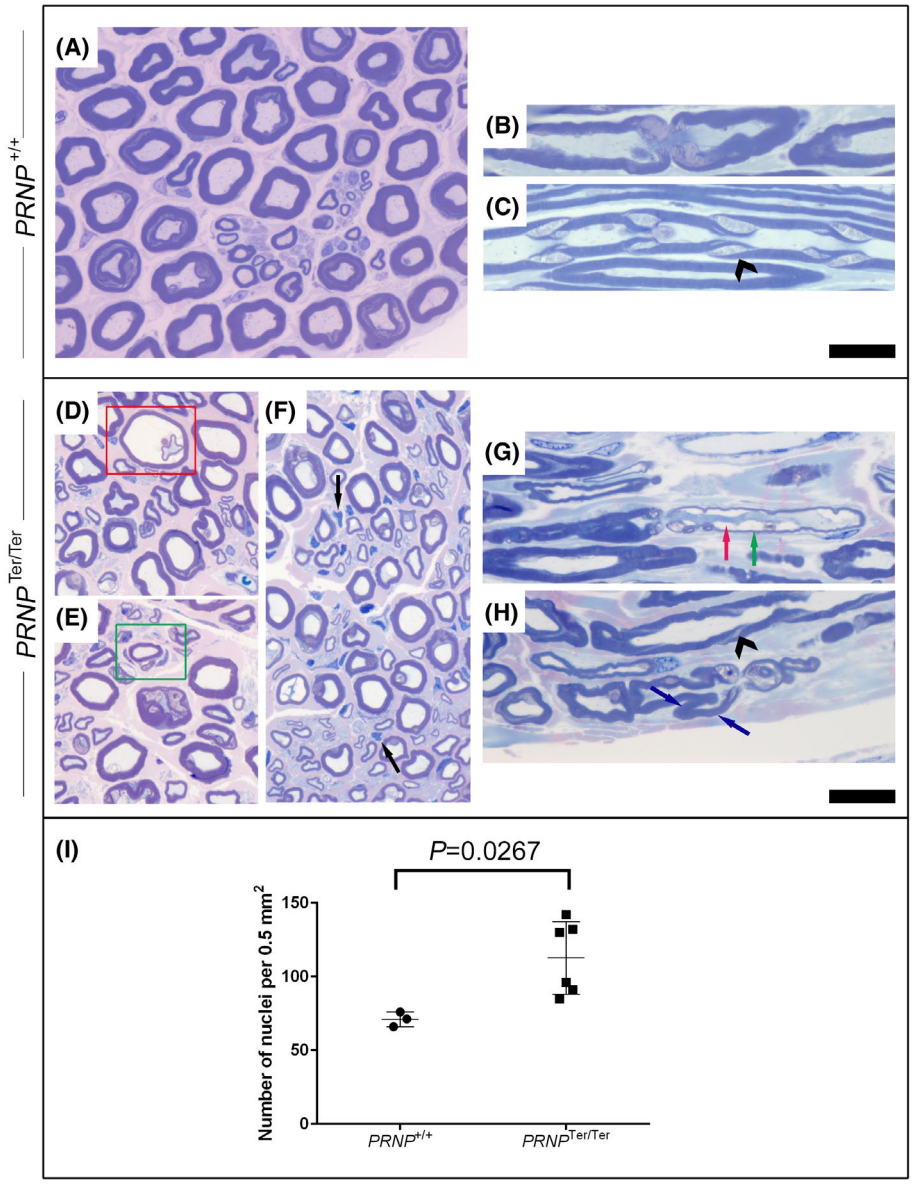

FIGURE 3 Toluidine blue- and safranin O-stained cross and longitudinal semi-thin sections of tibial nerves of $PRNP^{+/+}$ A-C, and $PRNP^{Ter/Ter}$ (D-H) goats. (C, H) Prominent Schmidt-Lanterman clefts were visible in both groups (arrowheads). D, Vacuolated fibers (red frame) were present in the nerves from the $PRNP^{Ter/Ter}$ goats; a fiber with severe myelin splitting and a shrunken axon centrally is shown in a red frame—compare with Figure 5A. E, A green frame shows an onion bulb. F, An increased number of cell nuclei (two examples are indicated by black arrows) was present in the nerves from the $PRNP^{Ter/Ter}$ goats. G, A remyelinated nerve fiber (green arrow) with swelling of the adaxonal Schwann cell cytoplasm (red arrow) is present next to an internode with normal myelin thickness. H, A paranodal outfolding (blue arrows) is visible next to a node of Ranvier. Bar 20 µm. I, Quantification of nuclei in semi-thin sections demonstrated increased number of cells in $PRNP^{Ter/Ter}$ goats

3.2 | Nerve fiber diameter distribution

We investigated nerve fiber distribution in $PRNP^{+/+}$ and $PRNP^{Ter/Ter}$ goats, and observed a lower percentage of large fibers in the latter group (Figure 7A). To compare myelin thickness between the groups, we calculated the *g*-ratio (axonal diameter/total fiber diameter) in cross sections of the tibial nerve. Nerve fibers from $PRNP^{Ter/Ter}$ goats had a higher *g*-ratio ($P = .0139$) than $PRNP^{+/+}$ goats (Figure 7B), particularly prominent in large myelinated fibers.

3.3 | Peripheral nerve lipid composition

Analysis of the peripheral nerve lipid composition was performed with UPC2-MS/MS technology enabling both high resolution detection of individual lipid species and a semi-quantitative estimation of lipid class distribution in the extracts.[20] Principal component analysis revealed a predominantly age-dependent difference of the global lipid profiles with adult goats (more than 1 year old) clustering separately from young goats (Figure 8A). However, a clear

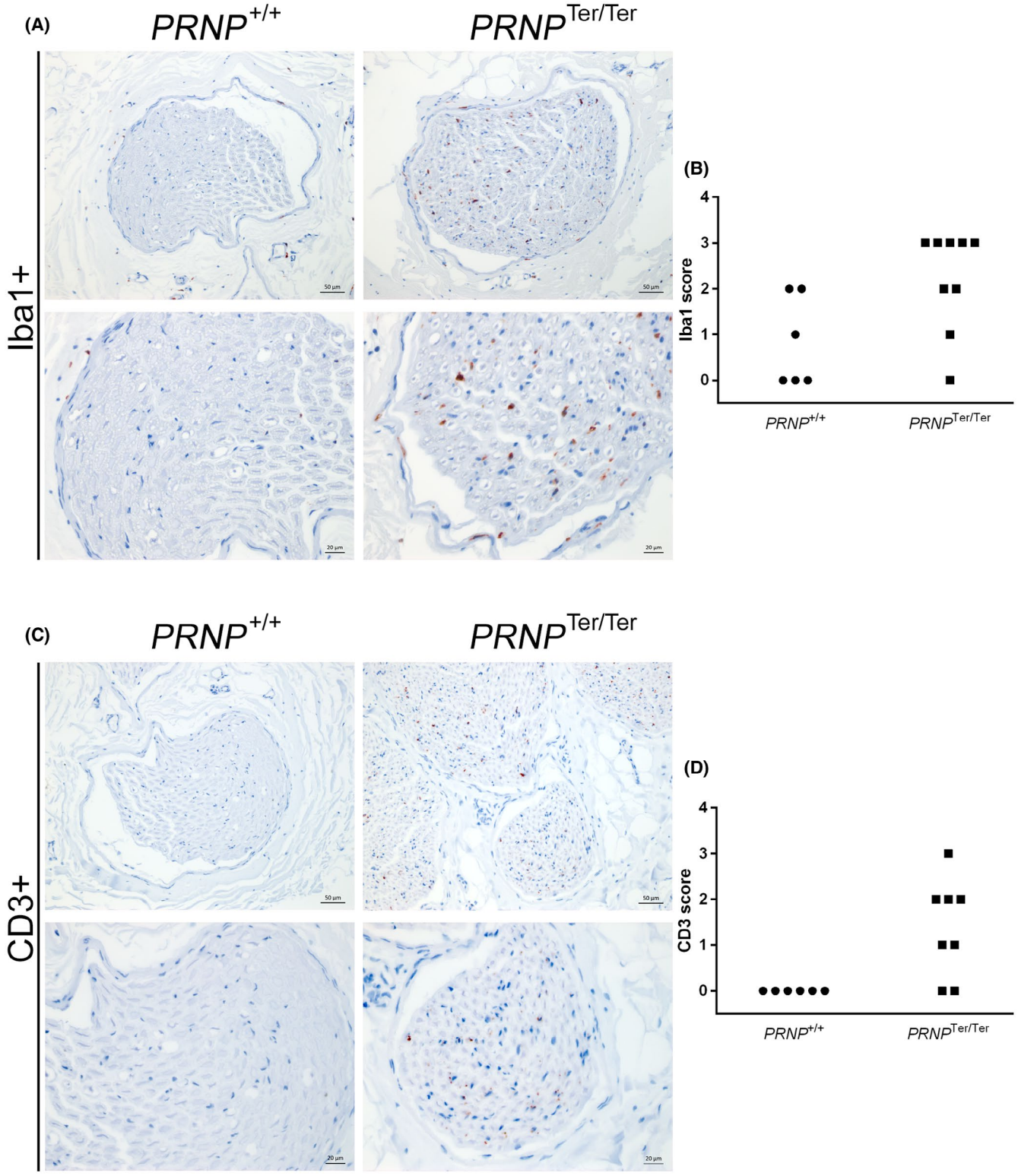

FIGURE 4 Immunostaining of Iba1+ (A) and CD3+ (C) cells in peripheral nerve cross sections. An increased level of Iba1+ cells in the endoneurium of *PRNP*$^{Ter/Ter}$ goats when compared to *PRNP*$^{+/+}$ indicates macrophage infiltration and/or proliferation in the former group. Endoneurial CD3+ lymphocytes are present in the *PRNP*$^{Ter/Ter}$ goats. In the *PRNP*$^{+/+}$ group, no signal was observed from the endoneurium. Quantification of the staining level was performed for both Iba1 (B) and CD3 (D), confirming increased staining in *PRNP*$^{Ter/Ter}$ goats

enrichment of hexosyl ceramides (HexCer) was observed among the lipids significantly changed within the adult groups. While only 13% of lipid species accounting for only 5% of summed abundance in the whole lipidome is significantly changed, 42% lipid species (44 out of 105 species) and 30% in summed abundance is significantly changed in

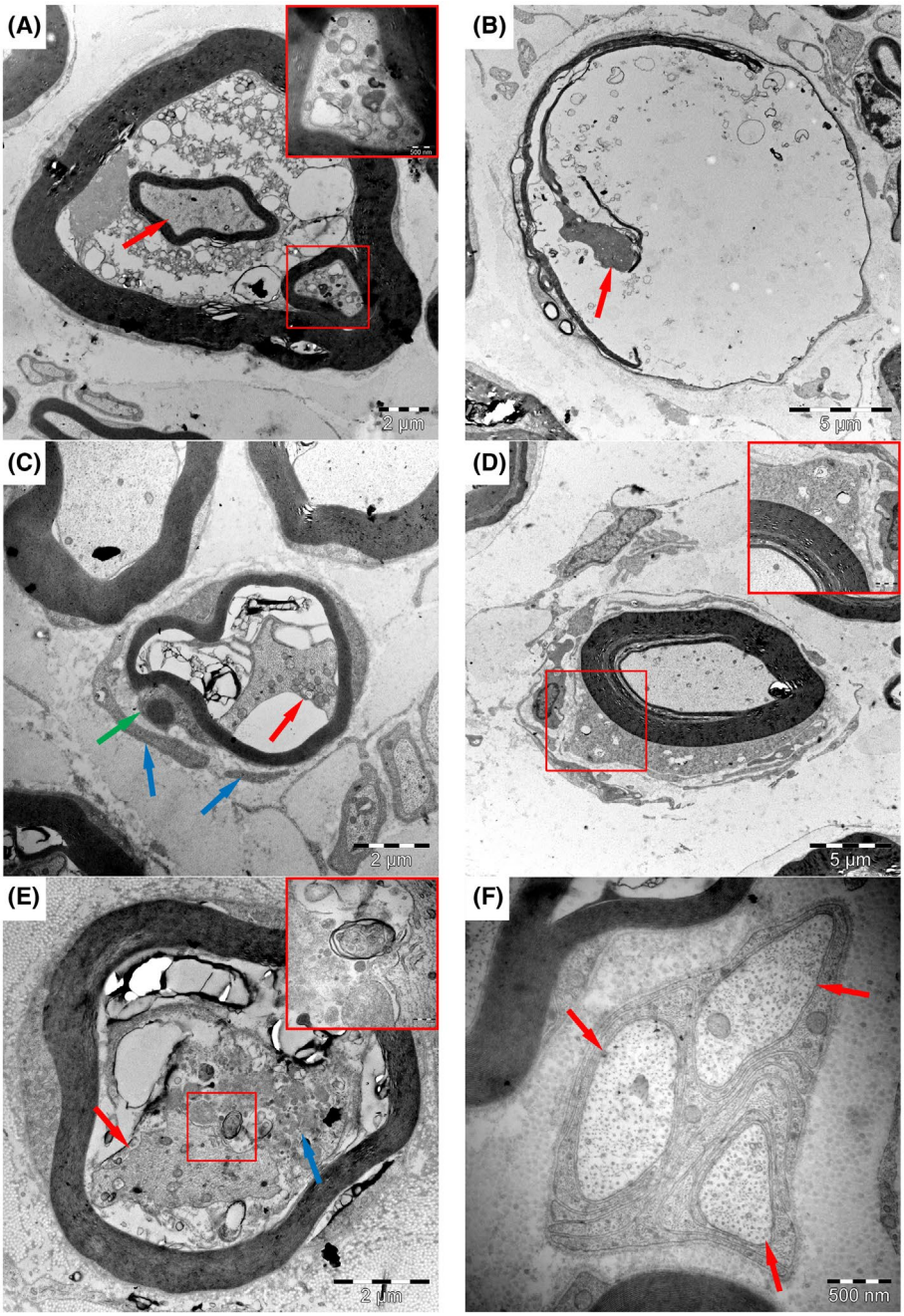

FIGURE 5 Ultrastructural changes in nerves from *PRNP*$^{Ter/Ter}$ goats. A, Myelin splitting and accumulation of vesicles. A shrunken axon (red arrow) is present in the middle of the image, while a myelin fold surrounds a cytoplasmic space with accumulation of mitochondria (red frame, magnified in inset). B, A severely swollen nerve fiber with a shrunken axon (red arrow). Only remnants of the myelin sheath are present. Vesicular structures are visible in the vacuolated space. C, An axon with abnormally thin myelin sheath is surrounded by supernumerary Schwann cell processes in a small onion bulb. The cytoplasm of the myelinating Schwann cell is indicated by green arrow, while the supernumerary Schwann cell is shown with blue arrows. The axon is shrunken and has increased densities of neurofilaments and mitochondria (red arrow). D, Cellular infiltrates next to a myelinated fiber with prominent rough endoplasmic reticulum in the Schwann cell. E, Dysmorphic organelles (red frame, magnified in inset) in the adaxonal Schwann cell cytoplasm (blue arrow). Shrunken axon (red arrow). F, No changes were detected in unmyelinated fibers (red arrows) of a Remak bundle

the HexCer lipid class for the adult goats (Figure 8B). A closer inspection of the 18 most abundant species constituting 95% of the total abundance of the HexCer group revealed a global downregulation of HexCer of the *PRNP*$^{Ter/Ter}$ goats compared to the adult controls (Figure 8C). There were individual differences, that is, goats 1, 2, 3, and 5 are down in all HexCer lipids, while goats 4 and 6 still have a more scattered abundance profile, probably reflecting that the demyelination has reached different stages among the *PRNP*$^{Ter/Ter}$ goats.

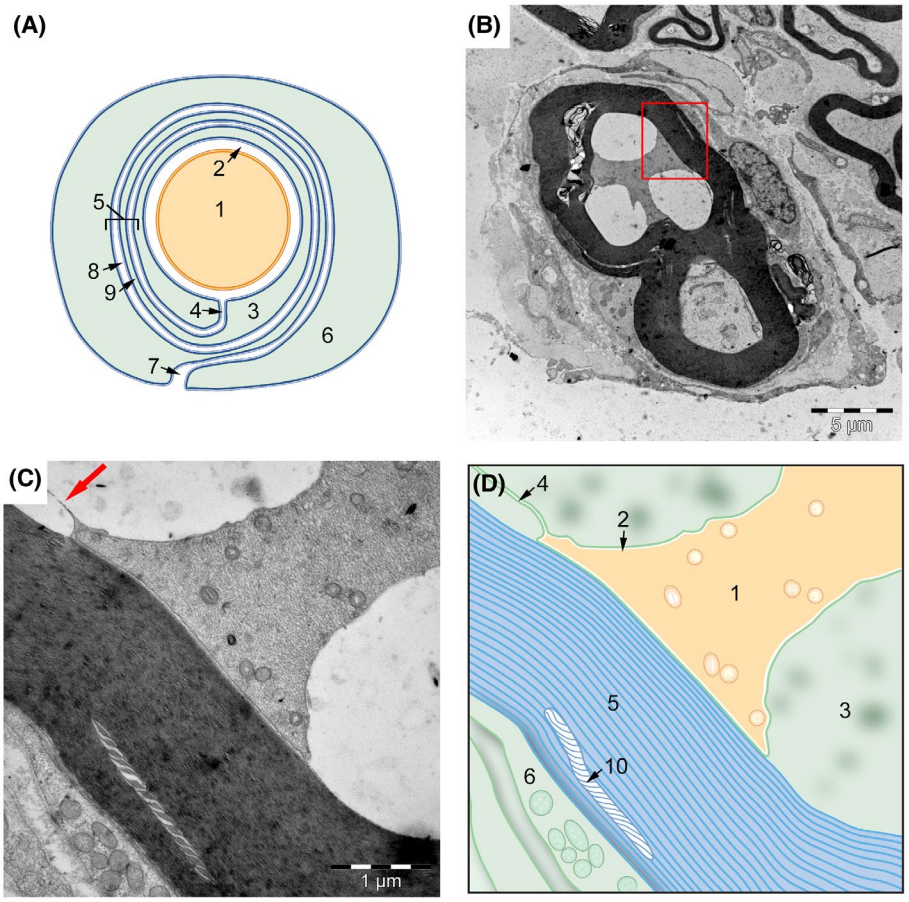

FIGURE 6 A, Schematic representation of a myelinated fiber. B, A myelinated nerve fiber with swelling of the adaxonal Schwann cell cytoplasm (red frame in b, magnified in C, Note the presence of vesicular structures in the adaxonal Schwann cell cytoplasm. The inner mesaxon is indicated by the red arrow. D, Schematic representation of c. 1 = Axon, 2 = Periaxonal space, 3 = Adaxonal Schwann cell cytoplasm, 4 = Inner mesaxon, 5 = Compact myelin, 6 = Abaxonal Schwann cell cytoplasm, 7 = Outer mesaxon, 8 = Intraperiod line, 9 = Major dense line, and 10 = Schmidt-Lanterman cleft

3.4 | Genomic analysis

The average minor allele frequency across the 29 autosomes showed strong similarity between the AI bucks (n = 41) and the group of individuals heterozygous (n = 33) for the *PRNP*^{Ter} allele. The goats homozygous for the *PRNP*^{Ter} allele (n = 20) had a lower MAF across all chromosomes, reflecting their increased relatedness relative to the general goat population. As expected, these homozygous goats also showed a significant drop in MAF at chromosome 13, on which *PRNP* resides, indicating an extended homozygosity surrounding the *PRNP* locus (Figure 9A).

A more detailed analysis of chromosome 13 was achieved by plotting the average MAF of a sliding window of 5 SNPs across the chromosome. Only noncarriers and homozygous *PRNP*$^{Ter/Ter}$ goats were plotted (Figure 9B,C). These data show that 58 consecutive SNPs in the region from 44.97 MB to 47.45 MB are completely homozygous, delineating the minimum shared haplotype between the homozygous individuals in our study. The *PRNP* gene is located in the region 46.45-46.47 Mb on goat chromosome 13, almost in the middle of the homozygous region. Whereas the homozygous region constitutes approximately 2.5 MB of genomic DNA, the region spanning from 43.7 to approximately 50.0 MB (6.3 Mb of genomic DNA) showed a reduced MAF compared with the rest of chromosome 13. This means that genes located in this wider region (43.7-50.0 MB) have increased linkage to the *PRNP*^{Ter} allele, while genes in the core region (44.97-47.45 Mb) are completely linked to the *PRNP*^{Ter} variant in the investigated population. In Supplementary Table 2, genes located in the core flanking region are given.

3.5 | Detection of PrP^{C} in peripheral nerves

Immunofluorescence analysis of PrP^{C} (Mab 6H4) in longitudinal and cross-sections of peripheral nerves (Figure 10) demonstrated that *PRNP*$^{+/+}$ goats showed a strong PrP^{C} expression in Schwann cells and myelin sheaths. Axons

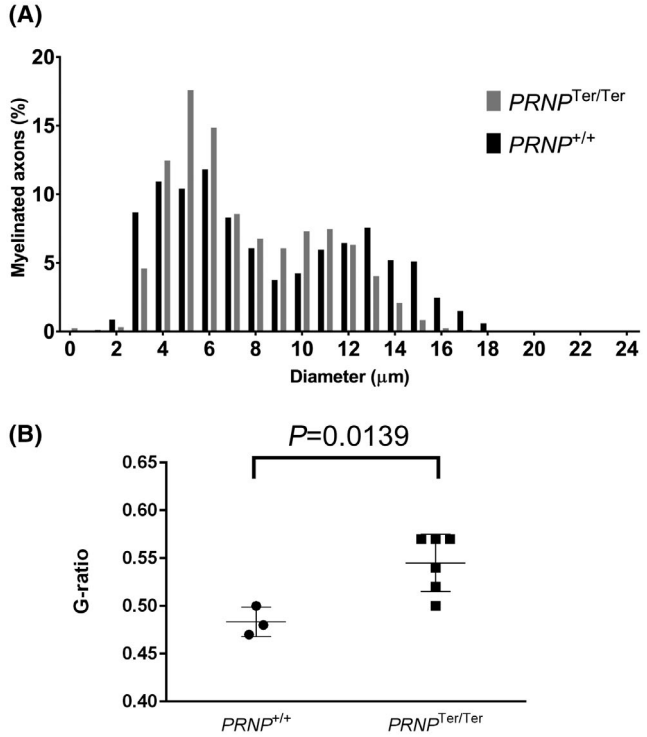

FIGURE 7 Fiber diameter frequency distribution in *PRNP*$^{+/+}$ and *PRNP*$^{Ter/Ter}$ A, goats illustrates a bimodal distribution in both genotypes and a loss of large diameter fibers in the *PRNP*$^{Ter/Ter}$ group. B, Nerve fibers of *PRNP*$^{Ter/Ter}$ goats showed a higher *g*-ratio (axonal diameter/fiber diameter), corresponding to a higher percentage of thinly myelinated fibers

appeared negative, but levels could be below the detection limit of the method used. As expected, PrP^{C} was not present in *PRNP*$^{Ter/Ter}$ goats. (Figure 11), western blot analysis confirmed PrP^{C} presence in *PRNP*$^{+/+}$ goats. Glycosylated full-length PrP^{C} is visible; moreover, after deglycosylation with PNGase-F, full length appeared at 27 kDa. A second band, with an approximate molecular mass of 22 kDa, could represent a C-terminal truncated form of PrP^{C}.

3.6 | Electrophysiology and clinical examination

Electrophysiological recordings are summarized in Supplementary Table 3. No significant differences in terms of latency were noted. No neurological deficits were observed in goats clinically examined.

4 | DISCUSSION

Over the past 7 years (from 2012), we have studied a total of nearly 50 homozygous *PRNP*$^{Ter/Ter}$ goats, both genders represented. Most have been young, but a few were more than 5 years old, and thus "aged" after husbandry standards. Although, no major physiological disturbances were apparent at rest, when subjected to acute endotoxin challenge, young (7 months) homozygous *PRNP*$^{Ter/Ter}$ goats displayed more profound sickness behavior[24] and increased inflammatory lung damage than normal goats.[25]

In the current study, analysis of peripheral nerves from goats, 8 months-7 years of age, revealed the presence of thinly myelinated internodes intermingled with internodes of normal myelin thickness, together with an increased variability in internodal length. These results suggest the presence of demyelinating neuropathy. These patterns of changes are in line with abnormalities observed at around 10 weeks of age in mice lacking the prion protein.[8-10] Axonal and not Schwann-cell restricted PrP^{C} expression completely prevented peripheral neuropathy in these mice, although some disease features were partly reversed after Schwann cell PrP^{C} expression.[10] Focally folded myelin was observed in the paranodal areas of the nerves of *Prnp*$^{-/-}$ mice.[10] Although paranodal demyelination is an early and unspecific sign of demyelination, the presence of intercalated internodes at both sides of a longer internode, as well as the severely dysmorphic paranodes in the *PRNP*$^{Ter/Ter}$ goats, could be due to a function for PrP^{C} in paranodal and juxtaparanodal fiber segments, in particular membrane junctions. In some nonneural tissues, like the gastrointestinal tract[26] and lungs,[27] PrP^{C} expression has been associated with stability of desmosomes, adherens junctions, and tight junctions. As the paranodal regions are stabilized by autotypic tight junctions,[28] one possibility is that in the absence of PrP^{C}, these are slightly destabilized, leading to paranodal outfoldings. Furthermore, disrupted axoglial junctions have been shown to cause ion channel dispersion with accumulation of potassium between the axon and Schwann cell, eliciting swelling of the Schwann cell and remodeling of the myelin,[29] a phenomenon that fits with the observed pathology in the nerves from *PRNP*$^{Ter/Ter}$ goats.

No clinical manifestations or electrophysiological aberrations were detected in *PRNP*$^{Ter/Ter}$ goats up to 7 years old. In *Prnp*$^{-/-}$ mice, reduced performance was noted in two out of three tests for neuromuscular function and nerve conduction velocity was also reduced, most pronounced at older age.[10]In this study, the oldest homozygous *PRNP*$^{Ter/Ter}$ goat was close to 7 years and appeared neurologically normal. However, goats can reach 15 years, so a seven-year-old goat is probably "middle-aged."

The pathophysiological significance of the elevated number of Iba1+ macrophages in the endoneurium of PrP-deficient goats needs further study. For instance, the macrophages appear to be evenly distributed throughout the endoneurium, and not, as in *Prnp*$^{-/-}$ mice, located to digestive chambers,[10] which are sites of myelin degradation. This raises the intriguing possibility that macrophage infiltration in goats precedes demyelination. To clarify

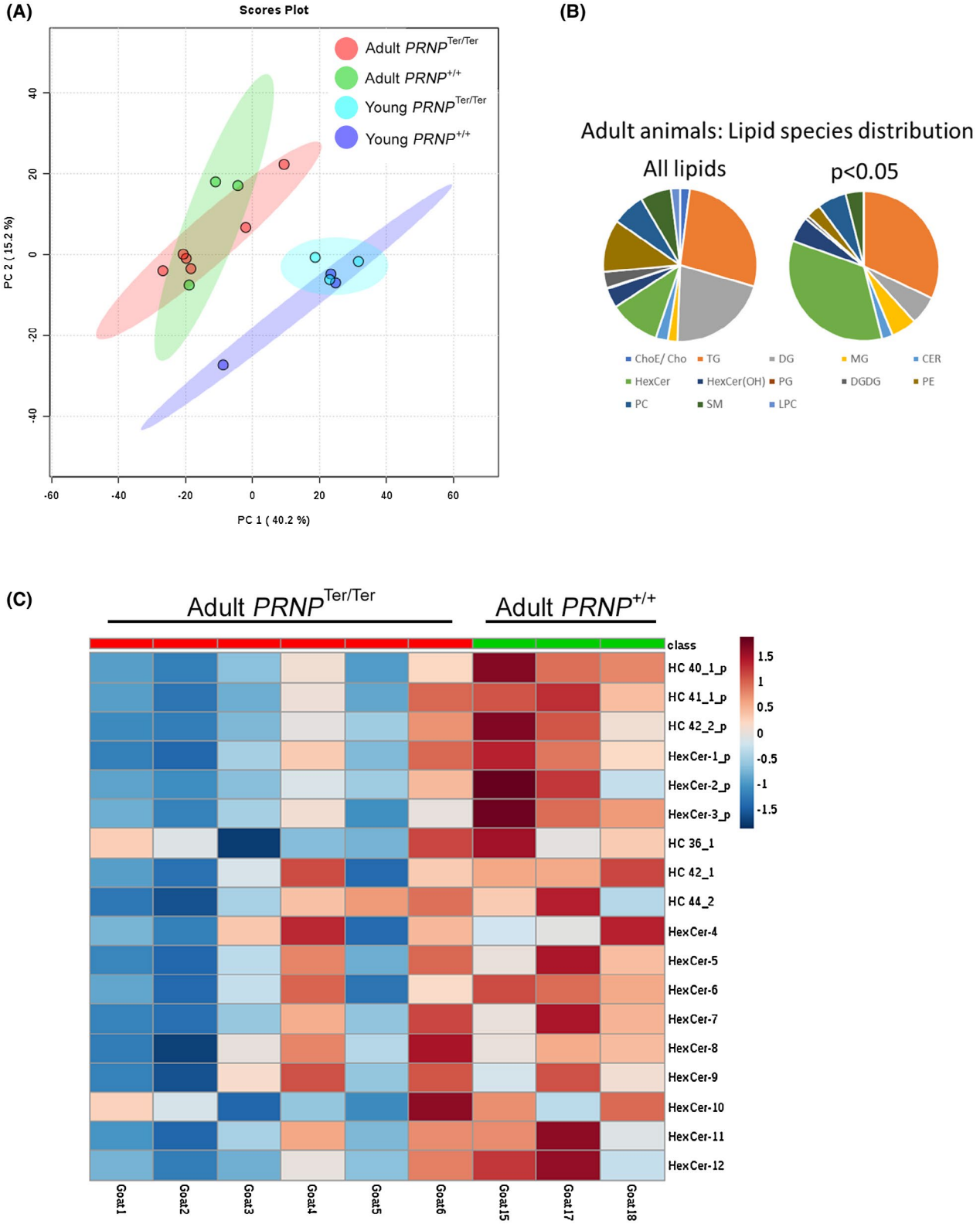

FIGURE 8 UPC^2-MS/MS analysis of peripheral nerve lipid composition. A, Principal component analysis (PCA) shows a clustering of animals according to age. B, Almost 1000 lipid species were retained after removal of noise and retention time filtering, and 128 of those were significantly changed between the two adult groups (*t*-test, $P < .05$). Of the 13 lipid classes (see Supplementary Table S4 for names), the hexosyl ceramides are enriched among the significantly changed (right panel in b and Supplementary Table S4). C, Nonordered heatmap presentation of the 18 most abundant HexCer lipids (top 6 with $P < .05$). Six of the lipids were tentatively identified with LipidMaps

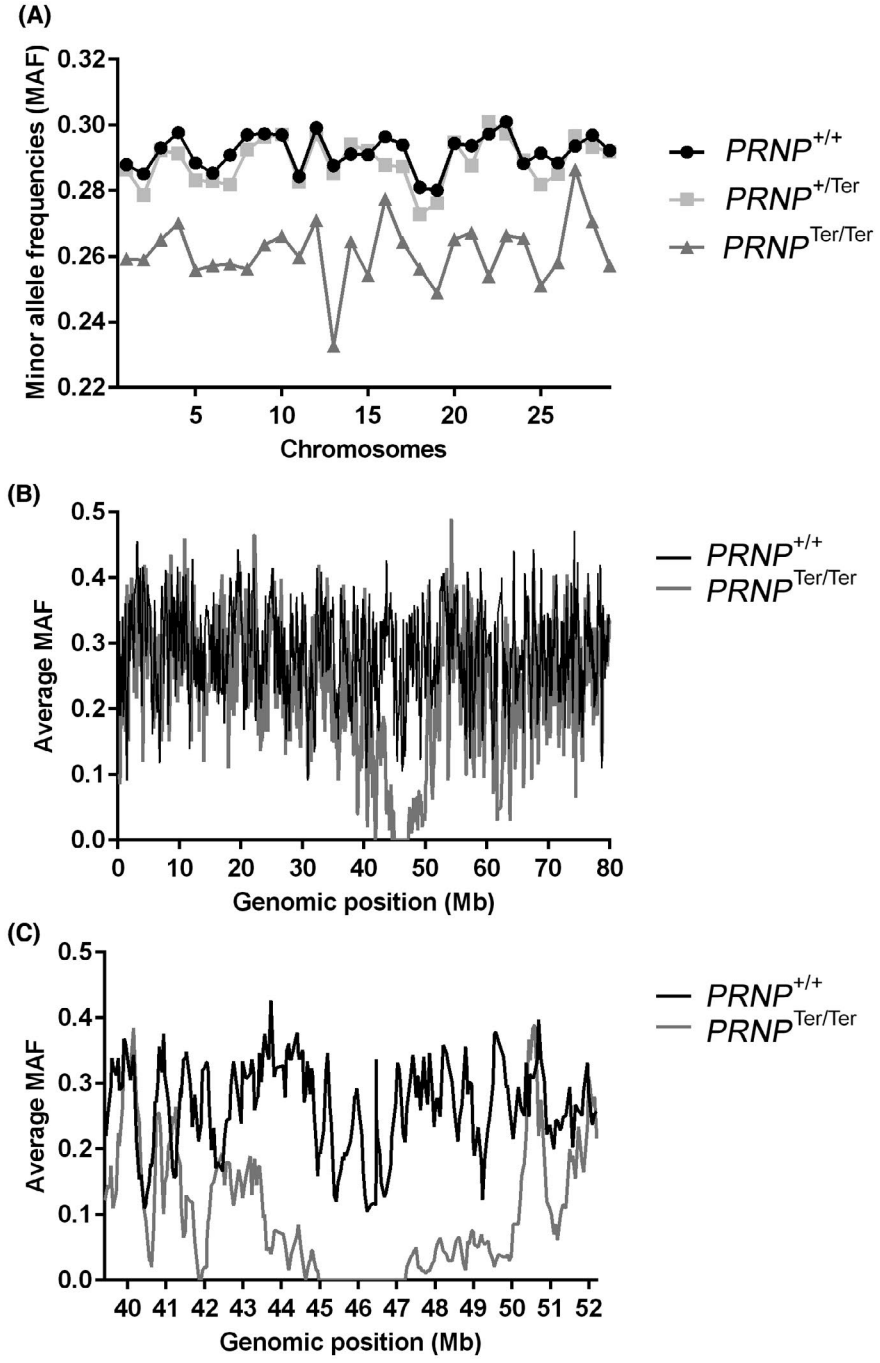

FIGURE 9 Haplotype analysis of goats. A, The figure illustrates the average minor allele frequencies (MAF) of all 29 autosomes, in $PRNP^{+/+}$, $PRNP^{+/Ter}$, and $PRNP^{Ter/Ter}$ goats. Chromosome numbers are on the x-axis and MAF-frequency on the y-axis. B, The graph shows the average MAF of a sliding window of 5 sequential SNPs across chromosome 13. For clarity, only $PRNP^{+/+}$ and $PRNP^{Ter/Ter}$ goats are included. Figure C, is zoomed in at the region surrounding the *PRNP* gene. Positions in mega bases (MB) on the x-axis and average MAF-frequency (of 5 sequential SNPS) on the y-axis

this, studies of nerves from younger goats are necessary. However, no increase in Iba1+ macrophages has been observed in the choroid plexus of goats without PrP^{C},[24] arguing that a pathological process in the peripheral nerves provides the chemoattractant clues for macrophage influx. Interestingly, we did not detect macrophages penetrating the basal lamina of Schwann cells; as reported in macrophage-mediated demyelination,[30,31] and observed in $Prnp^{-/-}$ mice.

Additionally, T lymphocytes infiltrating the goat endoneurium were detected. In mice, demyelination appeared independent of lymphocytes, since crossing $Prnp^{-/-}$ mice with recombinase-1 ablated mice $Rag1^{-/-}$ that are devoid of functional B and T lymphocytes, did not affect the pathogenesis. Although, polyneuropathies are heterogeneous with respect to clinical manifestations and pathogenic mechanisms, dysregulated immune responses that trigger or aggravate the conditions are a frequent commonality. Given that a mild, but distinct, systemic immunological imbalance has been observed in goats without PrP^{C},[24,25,32] it cannot be ruled out that this also affects the immunological homeostasis of peripheral nerves and that this can underlie, or possibly aggravate, what appears to be a primary demyelinating condition.

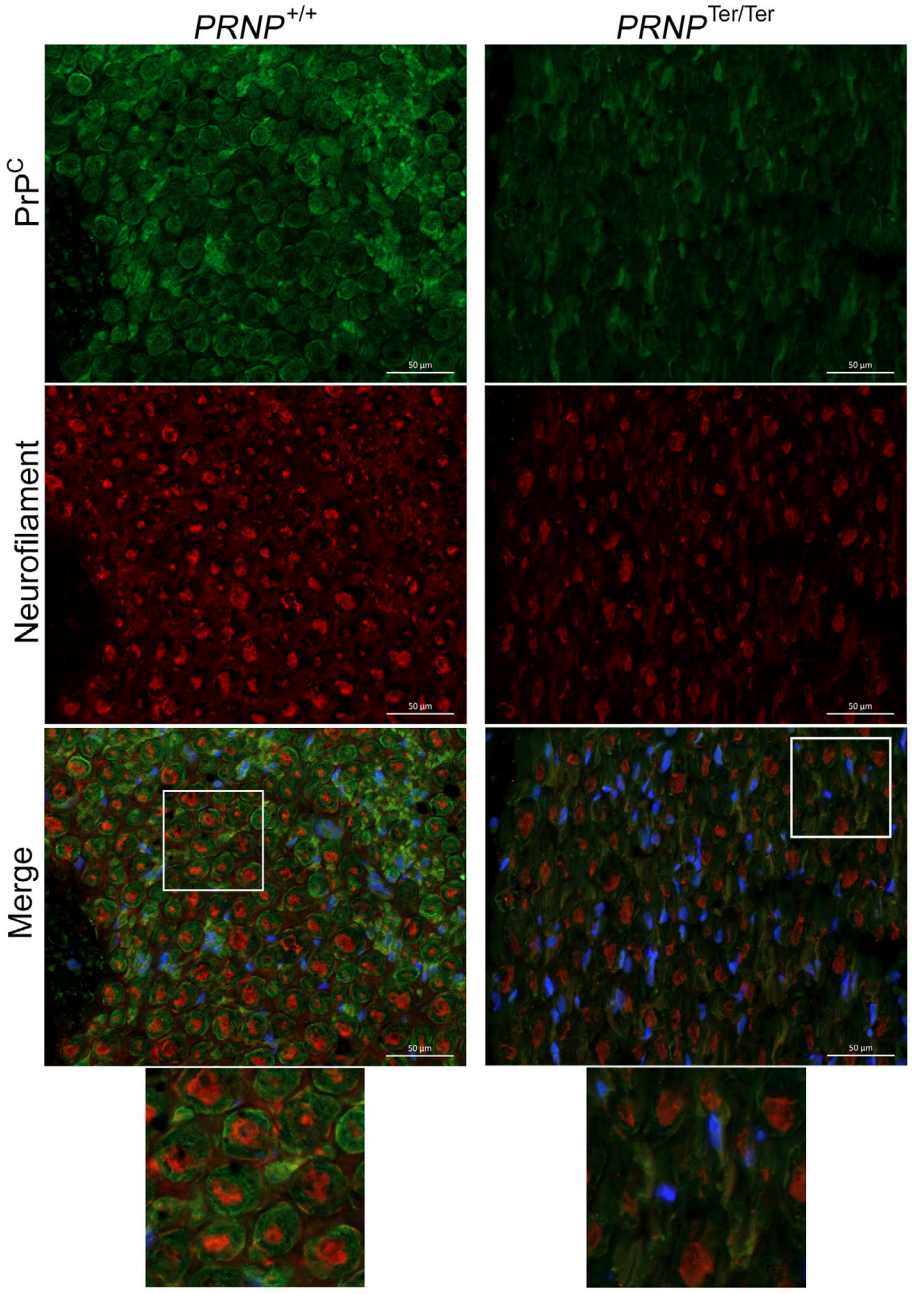

FIGURE 10 Localization of PrP^C in peripheral nerves. Immunofluorescence analysis of peripheral nerves in *PRNP*$^{+/+}$ (left) and *PRNP*$^{Ter/Ter}$ (right). PrP^C (green) is present in Schwann cells and compact myelin (magnification 40x, scale bars 50 µm.). Axonal neurofilament is stained red. White frames are magnified in the lower part of the figure

A contribution to myelin degeneration could arise from perturbation in lipid composition.[33] In goat nerves, we found that the lipid composition changes with age irrespective of *PRNP* genotype. Whereas no major differences due to genotypes were detected in young goats, changes in lipid composition between genotypes were evident in adults. Not all the lipid components differentially present were identified, but decreases in HexCer were noted. These lipids include galactosylceramides and glucosylceramides, and are among the sphingolipids. Mice lacking fatty acid 2-hydroxylase (FA2H), an enzyme involved in the synthesis of 2-hydroxylated sphingolipids, develop normally up to early adulthood, then develop degeneration in the spinal cord and lesions in the peripheral nerves, indicating that FA2H is necessary for myelin maintenance.[34] Glycosphingolipids are not essential for the synthesis of compact myelin, but are required for stability and maintenance of myelin into old age.[33] Whether or not PrP^C is involved in sphingolipid metabolism remains to be clarified.

Taken together, our results provide strong support for a PrP^C function in peripheral nerve myelin maintenance. Further studies that clarify the mechanisms by which PrP^C can affect myelin maintenance are needed. In vitro studies

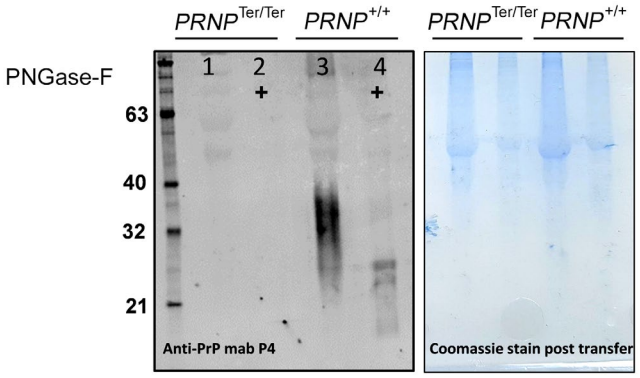

FIGURE 11 Western blot analysis of peripheral nerves. Glycosylated full-length PrP^C is detected in $PRNP^{+/+}$ goats. After deglycosylation with PNGase-F full length PrP^C is visible, together with a C-terminal fragment. No PrP^C was detected in $PRNP^{Ter/Ter}$ goats. On the right, Coomassie stain was used to verify equal protein loading between lanes

have shown that part of the amino-terminal flexible tail of PrP^C is released by proteolysis from axons and diffuses to a G protein-coupled receptor (Gpr126/Adgrg6), increasing cAMP levels in myelinating Schwann cells.[11] The binding of the flexible tail of PrP^C to Gpr126 has also been confirmed in vivo,[11] although the effect of Gpr126 on myelin maintenance has been questioned.[35]

Our genomic analysis of the *PRNP*-region at chromosome 13 shows that the invariant $PRNP^{Ter}$ haplotype only spans 2.5 Mb, which constitutes approximately 3% of the chromosome and less than 1% of the proteins encoded by chromosome 13. Thus, the haplotype containing the $PRNP^{Ter}$ allele are short compared with those observed in some of the $Prnp^{-/-}$ lines of mice.[36] Taken together, data from transgenic mice and the nontransgenic goat model presented here, demonstrate that PrP^C has a conserved role in myelin maintenance in mammals.

ACKNOWLEDGMENTS

The authors acknowledge Lucy Robertson for proofreading the manuscript, and Mari Katharina Aas Ådland for technical assistance.

CONFLICT OF INTERESTS

The authors declare that they have no conflicts of interests.

AUTHOR CONTRIBUTIONS

F.S. Skedsmo, G. Malachin, A. Espenes, and M.A. Tranulis designed the research. F.S. Skedsmo, G. Malachin, D.I. Våge, M.M. Hammervold, Ø. Salvesen, C. Ersdal, B. Ranheim, M.H. Stafsnes, Z. Bartosova, A. Espenes, and M.A. Tranulis performed the experiments. F.S. Skedsmo, G. Malachin, D.I. Våge, M.M. Hammervold, Ø. Salvesen, C. Ersdal, B. Ranheim, M.H. Stafsnes, Z. Bartosova, P. Bruheim, K.H. Jäderlund, K. Matiasek, A. Espenes, and M.A. Tranulis analyzed the data and wrote the paper.

REFERENCES

1. Prusiner SB. Molecular biology of prion diseases. *Science*. 1991;252:1515-1522.
2. Büeler H, Aguzzi A, Sailer A, et al. Mice devoid of PrP are resistant to scrapie. *Cell*. 1993;73:1339-1347.
3. Manson J, Clarke A, Hooper M, Aitchison L, McConnell I, Hope J. 129/Ola mice carrying a null mutation in PrP that abolishes mRNA production are developmentally normal. *Mol Neurobiol*. 1994;8:121-127.
4. Büeler H, Fischer M, Lang Y, et al. Normal development and behaviour of mice lacking the neuronal cell-surface PrP protein. *Nature*. 1992;356:577-582.
5. Sakaguchi S, Katamine S, Nishida N, et al. Loss of cerebellar Purkinje cells in aged mice homozygous for a disrupted PrP gene. *Nature*. 1996;380:528.
6. Moore RC, Redhead NJ, Selfridge J, Hope J, Manson JC, Melton DW. Double replacement gene targeting for the production of a series of mouse strains with different prion protein gene alterations. *Nat Biotechnol*. 1995;13:999.
7. Rossi D, Cozzio A, Flechsig E, et al. Onset of ataxia and Purkinje cell loss in PrP null mice inversely correlated with Dpl level in brain. *EMBO J*. 2001;20:694-702.
8. Nuvolone M, Hermann M, Sorce S, et al. Strictly co-isogenic C57BL/6J-$Prnp^{-/-}$ mice: a rigorous resource for prion science. *J Exp Med*. 2016;213:313-327.
9. Nishida N, Tremblay P, Sugimoto T, et al. A mouse prion protein transgene rescues mice deficient for the prion protein gene from purkinje cell degeneration and demyelination. *Lab Invest; A J Tech Methods Pathol*. 1999;79:689-697.
10. Bremer J, Baumann F, Tiberi C, et al. Axonal prion protein is required for peripheral myelin maintenance. *Nat Neurosci*. 2010;13:310-318.
11. Küffer A, Lakkaraju AKK, Mogha A, et al. The prion protein is an agonistic ligand of the G protein-coupled receptor Adgrg6. *Nature*. 2016;536:464.
12. Dyck PJ, Karnes J, Lais A, Lofgren EP, Stevens JC. Pathologic alterations of the peripheral nervous system of humans. In: Dyck PJ, Thomas PK, Lambert EH, Bunge R, eds. *Peripheral Neuropathy*. Vol 1. Philadelphia: WB Saunders; 1984:790-793.
13. Folch J, Lees M, Sloane Stanley G. A simple method for the isolation and purification of total lipides from animal tissues. *J Biol Chem*. 1957;226:497-509.
14. Lisa M, Holcapek M. High-throughput and comprehensive lipidomic analysis using ultrahigh-performance supercritical fluid chromatography-mass spectrometry. *Anal Chem*. 2015;87:7187-7195.
15. Fahy E, Subramaniam S, Murphy RC, et al. Update of the LIPID MAPS comprehensive classification system for lipids. *J Lipid Res*. 2009;50:S9-S14.
16. Liebisch G, Vizcaíno JA, Köfeler H, et al. Shorthand notation for lipid structures derived from mass spectrometry. *J Lipid Res*. 2013;54:1523-1530.
17. Purcell S, Neale B, Todd-Brown K, et al. PLINK: a tool set for whole-genome association and population-based linkage analyses. *Am J Human Genet*. 2007;81:559-575.

18. Kind T, Liu K-H, Yup Lee D, DeFelice B, Meissen JK, Fiehn O. LipidBlast - in-silico tandem mass spectrometry database for lipid identification. *Nat Methods*. 2013;10:755-758.
19. Fahy E, Sud M, Cotter D, Subramaniam S. LIPID MAPS online tools for lipid research. *Nucleic Acids Res*. 2007;35:W606-W612.
20. Holcapek M, Cifkova E, Cervena B, Lisa M, Vostalova J, Galuszka J. Determination of nonpolar and polar lipid classes in human plasma, erythrocytes and plasma lipoprotein fractions using ultrahigh-performance liquid chromatography-mass spectrometry. *J Chromatogr A*. 2015;1377:85-91.
21. Chong J, Soufan O, Li C, et al. MetaboAnalyst 4.0: towards more transparent and integrative metabolomics analysis. *Nucleic Acids Res*. 2018;46:W486-W494.
22. Weller RO, Cervós-Navarro J. General pathology of peripheral nerves. In: Weller RO, Cervós-NavarroJ, eds. *Pathology of Peripheral Nerves*. London: Butterworths; 1977:61-89.
23. Mizisin AP, Shelton GD, Wagner S, Rusbridge C, Powell HC. Myelin splitting, Schwann cell injury and demyelination in feline diabetic neuropathy. *Acta Neuropathol*. 1998;95:171-174.
24. Salvesen Ø, Reiten MR, Espenes A, Bakkebo MK, Tranulis MA, Ersdal C. LPS-induced systemic inflammation reveals an immunomodulatory role for the prion protein at the blood-brain interface. *J Neuroinflammation*. 2017;14:106.
25. Salvesen Ø, Reiten MR, Kamstra JH, et al. Goats without prion protein display enhanced proinflammatory pulmonary signaling and extracellular matrix remodeling upon systemic lipopolysaccharide challenge. *Front Immunol*. 2017;8:1722.
26. Petit CSV, Besnier L, Morel E, Rousset M, Thenet S. Roles of the cellular prion protein in the regulation of cell-cell junctions and barrier function. *Tissue Barriers*. 2013;1:e24377-e24377.
27. Kouadri A, El Khatib M, Cormenier J, et al. Involvement of the prion protein in the protection of the human bronchial epithelial barrier against oxidative stress. *Antioxid Redox Signal*. 2019;31(1):59–74.
28. Poliak S, Matlis S, Ullmer C, Scherer SS, Peles E. Distinct claudins and associated PDZ proteins form different autotypic tight junctions in myelinating Schwann cells. *J Cell Biol*. 2002;159:361-372.
29. Rodionova NN, Allakhverdiev ES, Maksimov GV. Study of myelin structure changes during the nerve fibers demyelination. *PLoS ONE*. 2017;12:e0185170.
30. Brechenmacher C, Vital C, Deminiere C, et al. Guillain-Barré syndrome: an ultrastructural study of peripheral nerve in 65 patients. *Clin Neuropathol*. 1987;6:19-24.
31. Prineas JW. Pathology of the Guillain-Barré syndrome. *Ann Neurol*. 1981;9(Suppl):6-19.
32. Malachin G, Reiten MR, Salvesen Ø, et al. Loss of prion protein induces a primed state of type I interferon-responsive genes. *PLoS ONE*. 2017;12:e0179881.
33. Schmitt S, Castelvetri LC, Simons M. Metabolism and functions of lipids in myelin. *Biochimica et Biophysica Acta (BBA)-Mol Cell Biol Lipids*. 2015;1851:999-1005.
34. Zöller I, Meixner M, Hartmann D, et al. Absence of 2-hydroxylated sphingolipids is compatible with normal neural development but causes late-onset axon and myelin sheath degeneration. *J Neurosci* 2008;28:9741-9754.
35. Mogha A, Harty BL, Carlin D, et al. Gpr126/Adgrg6 has Schwann cell autonomous and nonautonomous functions in peripheral nerve injury and repair. *J Neurosci*. 2016;36:12351-12367.
36. Nuvolone M, Kana V, Hutter G, et al. SIRPalpha polymorphisms, but not the prion protein, control phagocytosis of apoptotic cells. *J Exp Med*. 2013;210:2539-2552.

SUPPORTING INFORMATION

Additional supporting information may be found online in the Supporting Information section.

How to cite this article: Skedsmo FS, Malachin G, Inge Våge D, et al. Demyelinating polyneuropathy in Goats lacking Prion Protein. *The FASEB Journal*. 2020;00:1–17. https://doi.org/10.1096/fj.201902588R